Design and Implementation of Data Usability Processor into an Automated Processing Chain for Optical Remote Sensing Data

Erik Borg[1], Bernd Fichtelmann[1(✉)], Christian Fischer[2], and Hartmut Asche[3]

[1] German Aerospace Center, German Remote Sensing Data Center, Kalkhorstweg 53, 17235 Neustrelitz, Germany
{Erik.Borg, Bernd.Fichtelmann}@dlr.de
[2] German Aerospace Center, German Remote Sensing Data Center, Münchner Str. 20, 82234 Wessling, Germany
C.Fischer@dlr.de
[3] Department of Geography, University of Potsdam, Karl-Liebknecht-Strasse 24/25, 14476 Potsdam, Germany
gislab@uni-potsdam.de

Abstract. Diverse anthropogenic impacts will trigger worldwide environmental and social problems as e.g. climate change or social transformation processes. To observe these processes current information about status, direction of development and spatial or temporal dynamics of the processes are required. As the demand for current environmental information is increasing, earth observation (EO) and remote sensing (RS) techniques are moving to the focus of interest.

Generation and dissemination of RS based information products for e.g. time-critical applications can only be guaranteed by state-of-the-art concepts for data processing. This can be realized either by cumbersome and thus expensive interactive processing or by setting-up development and implementation of automated data processing infrastructure. In both cases information about data quality is important for the pre-processing and value adding processing steps. This contribution is focussed on a processor for automated data usability assessment which can be integrated into an automated processing chain adding information valuable for the user.

Keywords: Remote sensing · Processing chain · Data quality · LANDSAT

1 Introduction

Increasing scarcity of natural resources, such as fresh water or fertile soils, coupled with conflicting man-made pressures on land use results in potential risks for a sustainable development of natural environment and thus requires a careful use of limited resources. Hence, it is necessary to balance the different user requirements in order to

A.-L. Lamprecht (Ed.): ISoLA 2012/2014, CCIS 683, pp. 21–37, 2016.
DOI: 10.1007/978-3-319-51641-7_2

limit, and if possible, to reduce the increasing pressure on environment and its different land-cover and land-use classes. The knowledge of environmental parameters and the availability of geographic information are important prerequisites if progress is to be achieved on this issue successfully. To respond to global land-use conflicts the European Union (EU) and European Space Agency (ESA) have jointly initiated the COPERNICUS-programme, which is aiming in the development and provision of fundamental, accurate and reliable geo-information services based on RS data products and ancillary spatial data (e.g. in-situ-information) [1]. To establish a geo-data database a variety of state-of-the-art remote sensing (RS) technologies, including data from optical and radar satellite systems, have to be utilised.

Many geo- and biophysical parameters that are required for monitoring and/or modelling of environmental processes can only be derived by using optical RS. However, the quality of optical data depends substantially on the weather conditions at the time of data recording.

In cases of cloud-obscured optical data, interactive processing of sub-optimal datasets by an operator becomes inevitable. However, operator-based image evaluation and processing to extract geo- and biophysical parameters is time-consuming, requires considerable expertise, manpower, and, although defined visual interpretation defaults were met, each operator develops an own interpretation and assessment model. Thus, the results obtained for a given image can vary and under certain circumstances and the results are often not comparable. Especially, since the interactive visual data evaluation is very expensive, in many cases only cloud-free or nearly cloud-free data are preferred for an interactive data processing.

By using only optimal cloud-free data, the requirements of the COPERNICUS initiative for delivering value-added information products and environmental geo-services based on area-wide RS data cannot be fulfilled. This is only possible if all RS data, inclusive sub-optimal data, are processed. However, if those data are processed interactively the i. quality of value-added products cannot be standardised because by subjectivity of operators, and ii. manpower and time requirements of processing will significantly increase the production costs.

A solution for this problem is the development of an automated processing chain for sub- and /or optimal data at acceptable time and costs. This ensures the i. generation of usable quality products of bio- and geophysical information, ii. provision of area-wide value-added products for a given time or period, and iii. setup and control of automatic processing by choosing appropriate satellite data processing modules.

Relevant control parameters may include technical system parameters (gain and offset) as well as data acquisition parameters (acquisition time (scene centre scan time and/or start and stop of scan), geographical corner and/or centre coordinates, and sun azimuth and elevation angle of scene centre). Thus, meta-information on data quality is particular an important control parameter, for either choosing high-quality data for expensive interactive thematic processing or for event-driven control of automated pre-processing and thematic processing. This contribution focuses on data quality

parameter, that directly can be assessed from a given RS dataset and either can be expressed in terms of the cloud cover index[1] or the data usability index[2].

This paper deals with a data usability processor as part of an automatic processing chain. The processor supports data error assessment, calculation of geographical coordinates, and local time for real solar conditions of all image pixels. Furthermore, the provision of land-water information for quality assessment, the determination of cloud and haze coverage is shown, and the influence of cloud and haze distribution to data quality is discussed.

2 Materials and Methods

2.1 Data Basis

For developing the processing chain presented here 2,957 JPEG-compressed quick-look-data[3] with corresponding metadata[4] from the period of 2000 to 2003 have been used. A description of the preparation of the quick-look-data is given in [2, 3]. The procedure results in resampled bands of a ground resolution of 180 m and by using a JPEG-compression ratio of 10:1 [2] to minimize the storage volume. Although the level of compression depends on the image content of a RS scene, this represents a JPEG quality metric Q-factor of 35 [4].

2.2 Processing Chain

The European receiving station network for LANDSAT-7 comprises stations in Maspalomas (Spain), Kiruna (Sweden), Matera (Italy), and Neustrelitz (Germany).

These stations guarantee the receiving and storage of data on behalf of ESA and data processing is carried out in order of EURIMAGE [6][5]. Figure 1 shows a block diagram of the LANDSAT ground segment operated by the German Remote Sensing Data Center (DFD). The received data are processed and stored with subsequent metadata generated during the receiving phase [8]. The interactive processing step in the automatic processing chain is highlighted in red. At this point, data assessment is completed visually by interpreters using quick-look-data. The assessment framework for the interpretation was provided by ESA [9], covering the range from 0 = perfect usable to 90 = unusable and addresses criteria such as: i. artefacts (90 = unusable), ii. estimated haze, clouds, and cloud shade, iii. assessment of cloud distribution, iv. differentiation of clouds covering land or water, and v. estimation of data usability

[1] *Cloud Cover Degree:* Ratio of cloud pixels to total pixels of an unit (e.g. complete scene or quadrant of a scene).

[2] *Data usability:* Combination of cloud cover and cloud distribution as well as data errors.

[3] *Quick-look data* are preview images derived from original remote sensing data.

[4] *Metadata* describe remote sensing data (e.g. satellite mission, orbit, track, frame).

[5] LANDSAT-7/ETM + data receiving were stopped at the end of 2003 [7].

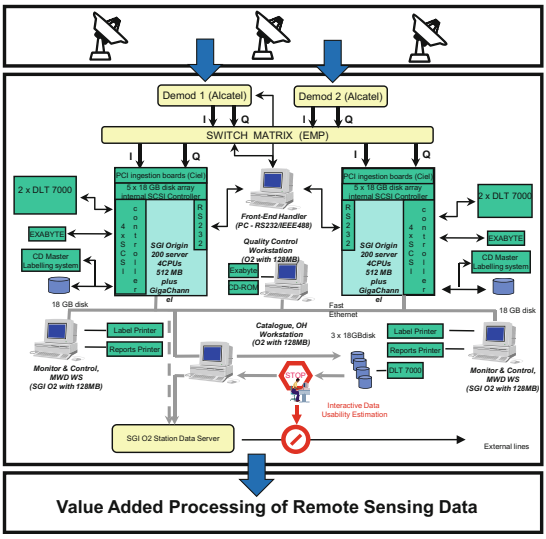

Fig. 1. Block diagram of the LANDSAT ground segment - red highlighted: interactive data usability assessment (adopted and changed from [5]). (Color figure online)

for land applications. The generated metadata and assessment results are then transferred to ESA [8].

3 Data Usability Processor for a Processing Chain

In addition to geographical and atmospheric data correction [10, 11] and the so called value adding (Fig. 2, left part) the development of the data usability processor for optical RS data can be integrated into the automated value added processing chain (adopted and changed from [12, 13]) (Fig. 2, right part).

Metadata[6] generated for the quick-look of Landsat-7/ETM+ data are essential to control the processing steps and for internal data transfer to the processor. The first processing step is to analyse the quick-look-data with respect to data errors, such as scan mirror errors, missing pixels, lines and areas [14].

If an erroneous data set is identified the data processing is terminated, otherwise the data is subjected to further processing by the cloud cover assessment (CCA) module, which is the processor core (right side in Fig. 2) and includes calibration, referencing to map in a usable projection and further classification by using sub-modules. The calibration module uses radiometric gain and offset, corner coordinates (based on preliminary Two-Line-Elements of satellite orbit) of the scene as well as equator crossing time to calculate at least sun elevation angle. These parameters are a pre-condition to

[6] *Meta-information:* Contain further information on remote sensing data (e.g. satellite mission, orbit, track, frame number, etc.).

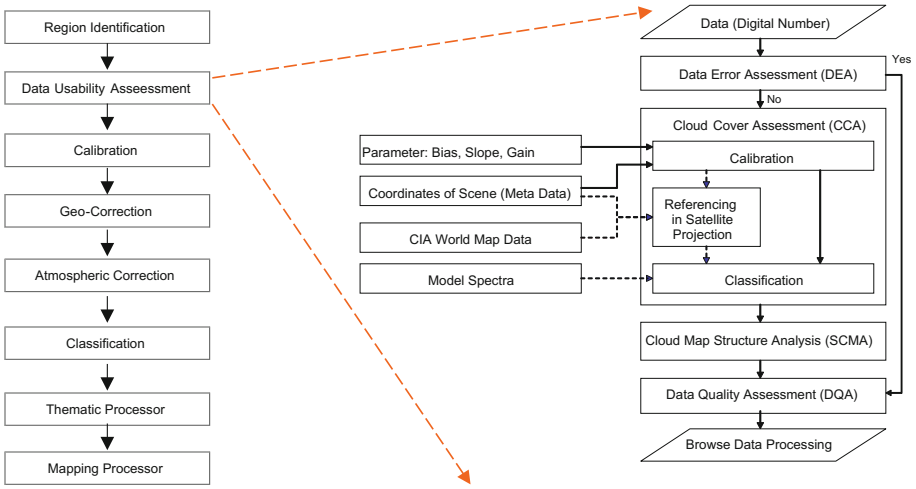

Fig. 2. Schematic diagram of a processing chain to derive value-added products (left) and integration of the developed data usability processor (right)

transform 8-bit observed uncalibrated raw data quantized in units of digital number (DN) to Top-of-the-Atmosphere (TOA) spectral radiance and after that into TOA reflectance for each pixel of optical bands, respectively, thermal band into surface temperature.

In the next processing step a land-water map is generated for the region of image data using geographical scene coordinates. The result of inverse geo-referencing of the land-water map to satellite image/quick-look data is subsequently used to control the cloud-haze-classification with respect to the background (land, water), and to optimise structure analysis in the quality assessment module (DQA).

For LANDSAT different classification algorithms are available [15, 16] facilitating the selection of an optimal processing module according to the target characteristics or geographic location.

The cloud-haze-mask allows the assessment of cloud cover degree of an image and it serves as an input for the subsequent cloud map structure analysis (SCMA). This module computes cloud distribution parameters for an assessment unit[7] (like a complete scene or a quadrant). The cloud cover and cloud distribution information are quality parameters for further processing [17].

These quality parameters are combined by using DQA in order to generate a data usability measure, whereas the cloud cover degree is a principal quality criteria and the cloud cover distribution is considered as an additional quality criteria to refine the data usability. Only this auxiliary criterion makes it possible to estimate the size of the usable image area [2].

[7] *Assessment unit:* scene, quadrant.

3.1 Pre-processing

Pre-processing of the data is an essential processing steps of the processor introduced here. The pre-processing subroutines include the following aspects (i) data error assessment, (ii) calibration, and (iii) transformation of topographic information into the original satellite image data. A short description of the different sub-processors is given in the following sections.

3.1.1 Data Error Assessment

According to ESA requirements [9], received imagery that is considered erroneous is excluded from further processing and is labelled as not further useable. Therefore, a reliable method for data error detection was developed [13]. The features used to distinguish both classes with high certainty are:

- Detection of erroneous lines or data sections showing only poor correlation with neighbouring undisturbed lines.
- Detection of erroneous image parts, lines or a number of pixels with *radiance = 0* in units of digital number (DN), characterizing the data as being unusable.

The preliminary test on selected erroneous LANDSAT-7/ETM+JPEG-compressed quick-look data have showed, that:

- missing lines cannot be identified with a high degree of confidence at very low sun angles,
- artefacts caused by the JPEG-compression led to a variety of false indications,
- computing time for determination of erroneous data sets is relatively high.

Therefore, a simplified method was developed which is based on the acceptance that erroneous pixel are characterized by *radiance = 0* in units of DN. The total number of such pixels is determined per line and tested against a threshold value of 10 pixels[8].

However, to minimize false indications, a threshold value was empirically derived for the identification of erroneous scenes. Moreover, the criterion 2 (*radiance = 0* in units of DN) proved to be adequate for the discrimination of disturbed and undisturbed data sets.

After data error analysis, usable data sets are provided to the next processing step while the other data are selected and labelled as non-usable.

3.1.2 Calibration

Calibration and transformation of LANDSAT-7/ETM+ data to TOA reflectance ρ and to effective at-sensor brightness temperature T [K] is described in detail by the LANDSAT-handbook [14]. Additional aspects which have to be considered for calibration is given by [17], computing planetary top of atmosphere reflectance ρ_p of band k based on digital number of a pixel (DN) [18, 19]. The relation to approximate Earth-Sun-distance d is given by [20].

[8] It has been shown that a threshold value of 10 is optimal because single zero-pixels are often caused by JPEG compression and were no data problem.

The transformation of pixel radiance in units of *DN* into planetary top of atmosphere reflectance ρ_p in a specified band k can be calculated by using Eq. (1) [14, 15, 18, 19]:

$$\rho_p = (\pi L(\lambda_k)d^2)/(E_S(\lambda_k)cos\Theta_S) \tag{1}$$

with: $L(l_k) = Gain(\lambda_k) * QCAL + Bias(\lambda_k)$, $L(l_k)$ spectral radiance at sensor's aperture $[W/(m^2sr\mu m)]$, Gain in $W/(m^2sr\mu m)/DN$, $QCAL$ the quantized calibrated pixel value in *DN*, *Bias* in $[W/(m^2sr\mu m)]$, $E_S(\lambda_K)$ mean exoatmospheric solar irradiance $[W/(m^2\mu m)]$, d Earth-Sun distance [*Astronomical Units*], and Θ_S solar zenith angle [*degrees*].

The transformation of spectral radiance in units of DN of thermal band 6 (wavelength: 10.4 µm to 12.5 µm) into at-sensor temperature T [K] can be calculated by using Eq. (2).

$$T = K_2/ln((K_1/L(l) + 1) \tag{2}$$

with: L_λ spectral radiance at the sensor's aperture $[W/(m^2sr\mu m)]$, K_1 calibration constant 1 $[666,09W/(m^2sr\mu m)]$[9], K_2 calibration constant 2 [*1282,71 K*][10].

3.1.3 Calculation of All Pixel Coordinates

The use of the solar zenith angle in Eq. (1) assumes at first that the geographic coordinates of all pixels are available. But only the corner coordinates of the scene are given for Landsat imagery, thus the coordinates for each individual pixel have to be calculated first. Additionally, the coordinates can be used to select topographic information for further data analyses.

The satellite orbit can be characterized in a static (non-rotation of Earth) geographical system Σ' using a reference track in a satellite system Σ, in which the track can be described only by length λ, while the latitude φ is 0 in every case. This satellite system is rotated by an angle $\delta = (180^\circ - \imath)$ ($\imath$ = inclination of the real orbit and reference satellite orbit in Σ') against the x-axis, which crosses exactly by ($\varphi = 0$, $\lambda = 0$), opposite to the geographical system.

The advantage of an equatorial orbit in system Σ is based on the fact that for a corresponding satellite image the distance between two points can be calculated with the relation (Eq. 3), assuming a spherical Earth piecemeal between the corner coordinates:

$$\begin{aligned} \varphi_1 &= \varphi_0 + i\Delta\varphi \\ \lambda_1 &= \lambda_0 + j\Delta\lambda \end{aligned} \tag{3}$$

[9] LANDSAT-handbook: chapter 9.2.4, Table 9.2 ETM+ Thermal Constants.

[10] LANDSAT-handbook: chapter 9.2.4, Table 9.2 ETM+ Thermal Constants.

where: $\Delta\varphi$ and $\Delta\lambda$ are the pixel size in latitude and longitude, respectively, and i and j are the distance of the two pixels in columns and lines.

The transformation of the coordinates φ and λ of system Σ into coordinates φ' and λ' of the geographical system Σ' is described by Eq. (4), where $r = r'$ [21]:

$$\begin{aligned} \cos\varphi'\cos\lambda' &= \cos\varphi\cos\lambda \\ \cos\varphi'\sin\lambda' &= \cos\delta\cos\varphi\sin\lambda - \sin\delta\sin\varphi \\ \sin\varphi' &= \sin\delta\cos\varphi\sin\lambda - \cos\delta\sin\varphi \end{aligned} \tag{4}$$

In each case, since the latitude of reference track is identical to geographical latitude of the real track in the geographical system, φ' can be considered as known. However, the coordinates of the track in Σ, defined by $\varphi = 0$, $\sin\varphi = 0$, and $\cos\varphi = 1$, are not given. But the coordinates for *UL, UR, LR,* and *LL* are known in the system Σ'. *UL* and *LL* are on parallel small circle track to satellite track, neglecting Earth rotation. The difference to longitude of *LL* is given by Earth rotation and will be calculated in one of the next steps.

The respective 4 geographical latitudes define the reference track in geographical coordinates. The corner coordinates on the left side of Eq. (4) and the angle δ on the right sight are known. The coordinates on the right side have to be determined to use at least Eq. (3) for determination of all pixel coordinates of the scene in system Σ. After that all coordinates in Σ can be transferred into the coordinate system Σ'. At least the deviation to the real track in the rotating system has to be determined.

The knowledge of the respective longitudes λ' is not necessary for the terms in line 3 of Eq. (4). The transformation of a small circle is sufficient for segmentation of an image in constant longitudes and latitudes sections. However, to transform the two left corner coordinates within Eq. (5) $\varphi = \varphi_G$ has to calculated as a prerequisite.

$$\lambda_k = arcsin[(sin\varphi_k - cos\delta sin\varphi_G)/(sin\delta cos\varphi_G)]; \quad \text{with}\, k = UL,\, LL \tag{5}$$

φ_G is given as latitude in the satellite system Σ and is the spherical distance between small circle and great circle, which represents the reference track. However, this distance is the same in every system Σ'. It is exactly half of the spherical distance of the two upper corner pixels which are located on the great circle. Pass the great circle (orthodrome) on a globe the points $A(\varphi_A, \lambda_A)$ and $B(\varphi_B, \lambda_B)$ the spherical distance α can be calculated to:

$$\alpha = arccos[sin\varphi_A - sin\varphi_B + cos\varphi_A cos\varphi_B cos(\lambda_B - \lambda_A)]; \quad A = UL,\, LL;\, B = UR,\, LR$$

For both pairs A, B the result is same with:

$$\varphi_G = \pm\alpha/2 \tag{7}$$

Knowing the difference of both longitudes when solving Eq. (5) for UL and LL and the corresponding line number n the line spacing $\Delta\lambda$ in Eq. (3) can be computed for the scene by Eq. (8).

$$\Delta\lambda = [(\lambda^0_{UL} - \lambda^{'}_{UL})/n]; \quad \text{with}\, n = \text{ line number} \tag{8}$$

The distance $\Delta\varphi$ (Eq. 3) between image elements of a line can be calculated using the pre-calculated spherical distance α for the borderline of the swath and the number of m image elements (columns) using Eq. (9):

$$\Delta\varphi = \alpha/m; \quad \text{with}\, m = \text{ column number} \tag{9}$$

The use of m and n assume, that under specific cases the coordinates of the *UL* corner corresponds the upper left corner of the *UL* pixel. In this case, it is necessary to include $\Delta\varphi\,/2$ and $\Delta\lambda\,/2$ in Eq. (3). If the centre of the *UL* pixel is given as upper left corner of the scene $(n-1)$ and $(m-1)$ have to be used in Eqs. (8) and (9).

A prerequisite for applying Eq. (9) is a scanning geometry with constant distance between line elements in Σ. In other case, the respective distance ($\Delta\varphi$ in Σ) between image elements has to be determined. Consequently the geometric assignment (φ, λ) for each image element of the appropriate reference track in the satellite system can be estimated by using Eq. (3).

Equation (4) is used for the transformation of coordinates (φ, λ) into geographical system Σ' with coordinates (φ', λ'). The third equation in (4) can be solved for φ'.

$$\varphi' = arcsin(sin\delta cos\varphi sin\lambda + cos\delta sin\varphi) \tag{10}$$

By using geographical longitude it has to be considered that the definition interval is given with $-180° < \lambda \leq 180°$. If a value or result of λ or λ' is outside this defined geographical interval, a back setting of this value will be executed by using Eq. (11):

$$\lambda_{red} = 2arctan(tan\ (\lambda/2)) \tag{11}$$

For the derivation of λ' the second equation in (4) is to divide by the first equation in (4).

$$(cos\varphi' sin\lambda')(cos\varphi' cos\lambda') = (cos\delta cos\varphi sin\lambda - sin\delta sin\varphi)/(cos\varphi cos\lambda) \tag{12}$$

After reducing and the introduction of the Tangency-function

$$\tan\lambda' = \cos\delta\tan\lambda - \sin\delta\tan\varphi/\cos\lambda \tag{13}$$

Equation (12) can be solved for λ'.

$$\lambda' = \arctan(\cos\delta\tan\lambda - \sin\delta\tan\varphi/\cos\lambda) \tag{14}$$

φ' and λ' are the coordinates of a satellite scene with an orbit defined in geographic coordinates $[\varphi^{'} = 0, \lambda^{'} = 0]$. After that, the image coordinates for the reference track in the geographical system Σ' with respect to the real coordinates in the rotating geographical system Σ' has to be calculated. By rotation around the z-axis (North-South axis of Earth) with:

$$\Delta\lambda_0 = ABS(\lambda^0_{UL} - \lambda^{'}_{UL}) \tag{15}$$

The reference image can be rotated in a way that the first line covers the first line in the original image, when placed in the system Σ'. λ^0_{UL} is the longitude of the available geographical *UL* corner coordinate and $\lambda^{'}_{UL}$ is the corresponding longitude of *UL* after its inverse transformation from Σ (results of Eqs. (5) and (7)).

All additional lines of the two images which correspond to each other are moved because of the earth rotation. This additional shift caused by the earth rotation $\Delta\lambda^0_j$ of each single image line can be computed with the help of the differences in the length of the two left real geographic corner coordinates $(\lambda^0_{UL}, \lambda^0_{LL})$ to the respective corresponding length $(\lambda^{'}_{UL}, \lambda^0_{LL})$ in the reference image:

$$\Delta\lambda^0_j = j * ABS((\lambda^0_{UL} - \lambda^{'}_{UL}))/n; \quad \text{n} = \text{number of lines} \tag{16}$$

The calculation of λ^0_{LL} is carried out accordingly to λ^0_{UL}, and by using $-\alpha/2$ in Eq. (7). The geographical latitude remains constant despite of earth rotation. The coordinates of the scene are completely available for all pixels after execution of the corrections of longitude λ':

$$\lambda^{''}_{i,j} = \lambda^{'}_{i,j} + \Delta\lambda_0 + \Delta\lambda^0_j); \quad \text{for all } i,j \tag{17}$$

3.1.4 Pixel-Based Local Time Calculation

The next subtask calculates local time for each pixel of the scene. It can be shown (e.g. [22]) that for a satellite with a sun synchronous orbit the local crossing time (LCT) t_{LC} for the respective nadir point of the satellite orbit can be derived in dependence of its geographical latitude φ_N and a constant local equator crossing time (LECT) t_{LEC} based on the previously already known parameters.

$$t_{LC} = t_{LEC} - arcsin(tan\ \varphi_N cot\imath)/15; \quad \imath = \text{inclination of track} \tag{18}$$

The minus '−' in Eq. (18) refers to the descending node of the track. A precondition for Eq. (18) is the correct knowledge about calculation of t_{LEC}. Johnson et al. [22, p. 12] are referring that "ignoring any long-term drift, the time of a satellite pass measured in local solar time at nadir, is constant for given latitude." The time of a satellite pass includes the crossing of equator.

In [23, 24] Eq. (19) is used for determination of LECT ($t_{LEC} = t_{LC}$ for points with geographic latitude $\varphi = 0$) for mean solar conditions.

$$t_L = t_{LC} = t_{GM} + \lambda_G/15 \tag{19}$$

where: t_{GM} is the time of equator crossing in Greenwich Mean Time, GMT (in hours) [23] or in Coordinated Universal Time, UTC (in hours) [24]. But a well-known

difference exists between Real and Mean Sun with the result that for instance local noon will change of −14 and +16 min within a year. This characteristic variation overlays the diurnal drift of equator crossing shown e.g. in [25] for NOAA-9 satellite.

By neglecting the orbit drift the time of equator crossing for Real Sun conditions will change in the same order within a year. This behaviour is caused by the elliptic orbit of Earth around sun and tilt of Earth's axis. This relation is described by the equation of time (t_E) which can be found e.g. in [26] and has to be considered as additional term on the right side of Eq. (19).

The Systems Tool Kit (STK) software [27] for orbit determination and the available two-line elements of LANDSAT-7 orbit were used to calculate t_{LEC} (in UTC) for each 21st day of the months for the year 2000. The simulated Real Sun t_{LEC} values (in hours) for the descending node are showing by asterisks in Fig. 3. Already with help of these 12 points is obvious, that the variation of t_{LEC} is similar to that of Equation of Time (t_E) [26]. Furthermore, if using Eq. (20) to determine t_{LEC} for Mean Sun a constant value was expected for LANDSAT satellite. But the difference between minimum and maximum of t_{LEC} for Mean Sun is around 2.5 min for the year 2000. The nearest t_{LEC} value to 10:06 a.m. (mean t_{LEC} of the 12 values) is given for 21st of June. If using the t_{LEC} and t_E for this date as basis (index 2106 in following equations), it is possible to describe the seasonal variation of t_{LEC} (in hours) in a first approximation with Eq. (20):

$$t_{LEC} = t_{LE2106} + (t_E + t_{E2106})/60; \quad (t_E, t_{E2106} \text{ in minutes}) \tag{20}$$

The effect of orbital drift has to be included into Eq. (20) additionally. The inclusion of t_{LEC} of Eq. (20) into Eq. (18) results in Eq. (21).

$$t_{LC} = t_{LEC\,2106} + (t_E + t_{E\,2106})/60 - arcsin(tan\varphi_N cot\imath)/15 \tag{21}$$

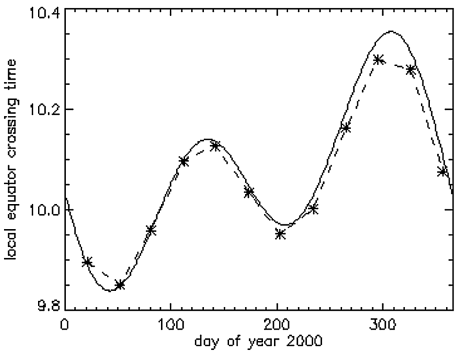

Fig. 3. Comparison of variation of t_{LEC} (in hours) for Real Sun determined for each 21st day of the month (year 2000 - dashed line) and simulated variation of t_{LEC} (in hours) determined by using Eq. (20) based on the defined reference point 21st June and equation of time computed for each day (year 2000 - solid line) for descending node of LANDSAT-7.

Equation (21) only applies to the nadir point of the satellite orbit. Therefore, the local time for all pixels of an image line have to be corrected by using their respective length difference $D\lambda'' = \lambda'' - \lambda''_N$ to the nadir point of this line by an additional term.

$$t_{LC} = t_{LEC2106} + (t_E + t_{E2106})/60 - arcsin(tan\varphi_N cot\imath)/15 + \Delta\lambda'' \Big/ 15 \tag{22}$$

Thus, the geographical latitude and longitude as well as the corresponding local time for each pixel are available to calculate the solar zenith angle Θ_S. It depends on season and local time and can be calculated as

$$\Theta_S = arccos(sin\delta_S sin\varphi' + cos\delta_S cos\tau cos\varphi') \tag{23}$$

where: φ' is the geographic latitude (Eq. 10), δ_S is the solar declination [26], and τ is the local time t_{LC} (Eq. 22) as angle.

3.1.5 Transformation of Topographic Information into Satellite Projection

Topographic information is an essential additional prerequisite for further automated processing (e.g. classification) of RS data. In cases of cloud-covered data it is useful to compare actual recorded data with a land-water mask to decide if clouds cover water or land e.g. in order to access the data usability for land applications.

As a rule for this, satellite data are corrected based on a topographical basis to make further processing of the data (e.g. atmospheric correction or thematic classification and value adding) possible. As a result of the transformation into the topographic projection the satellite image is larger, and consequently, triangles with no-data values on the four image borders will be generated (see Fig. 4b). This results in a decreasing performance of the processor.

Making very fast processing possible, the precursor procedure "Transformation of topographic Information into Satellite Projection" was developed and used here. The advantages are:

- A processor component is a structure analysis computing the connectivity of cloud pixels.
- A land-water mask is a binary image unlike the RS data. Therefore, a clear allocation can be carried out at the transformation of the data.

These considerations presupposed, the topographic data can be transformed into an image covering the satellite image data (hereafter referred as satellite projection[11]) as described in [28]. Each pixel of map has the same size as pixels of image. Figure 4 demonstrates schematically the operation steps for delivering the topographic information in satellite projection.

[11] The term Satellite Projection as it is used here is no projection in real sense of the word. A LANDSAT data track is resulting of sequential lines along the satellite path. Each line is a central projection from the satellite position.

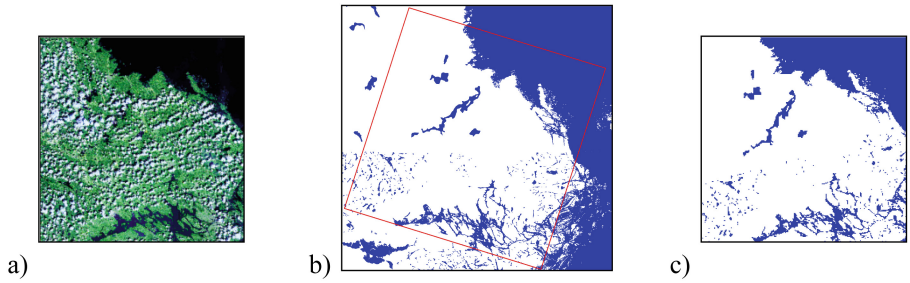

Fig. 4. Topographic information in satellite projection (blue: water; white: land) (adopted and modified by [28] (a) LANDSAT data (Stockholm-region 2002/06/01) (RGB: band 7, 5, 3). (b) Map in Lambert projection with inscribed region of quick-look-data as given in (a). (c) Resulting land-water mask after transformation (b) on basis of coordinates (as additional layer of satellite data). (Color figure online)

3.2 Value Added Processing

3.2.1 Classification of Quick-Look-Data

The aim of a classification scheme is based on grouping objects with the same feature properties to pre-defined criteria and the differentiation to other objects which do not show these feature properties.

The available methods for classification are distinguished in supervised and unsupervised methods which can be applied interactively or automatically to a given data set. The used classification procedures in the data usability processor operate automatically on a pre-defined classification scheme. The used LANDSAT-7/ETM + -classification schemes are the NASA-ACCA (NASA - National Aeronautics and Space Administration) [15] and the ACRES-ACCA-procedure (National Earth Observation Group - previously known as ACRES) [16]. The NASA-procedure was developed as a component of the operative processing chain of the LANDSAT ground station at EROS Data Center in Sioux Falls [15], while the ACRES-procedure was integrated in the operative LANDSAT-processing chain of ACRES [16].

The potential to process JPEG-compressed quick-look-data of both established automatic cloud cover assessment (ACCA) procedures were analysed by [3]. The results of the classification can be seen as satisfactory for the application to JPEG-compressed quick-look-data and the processing time is minimal.

3.2.2 Structure Analysis of Classified Data

The procedure used for analysing cloud deviation structure within an assessment unit and for deriving indicators to estimate the usability of RS data is described by [13].

Direction filters [29, 30] are used for the determination of the cloud distribution in the scene, to estimate in the eight predefined directions the distance of undisturbed pixels. The eight matrices for both the cloud mask and cloud-free comparison mask are the result of filtering. The minimal distance value is determined by use of a minimum operator and stored into a temporary result matrix for both masks. The results of the structure analysis are handed over to the sub-module for assessing the data usability value.

3.3 Value Adding LANDSAT-7/ETM + Data and Browse Mapped Products

Besides the data usability information for the quadrants, the procedure delivers for each image diverse selected technical and scientific parameters as browsable products. This is the final result of the data processing chain.

In addition, other information can be made available taking different requirements and various processing strategies of optical RS data into account. The results support an user in cases of search for optimal data in large remote sensing data archives.

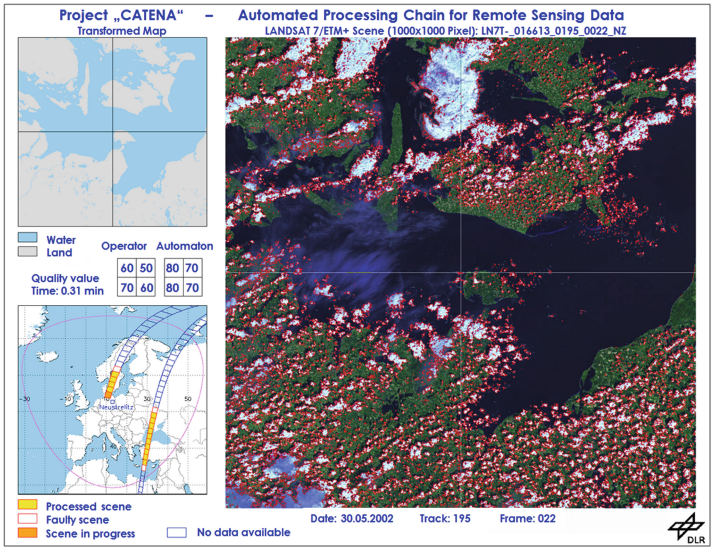

Fig. 5. Browse product to support interactive visual data quality assessment.

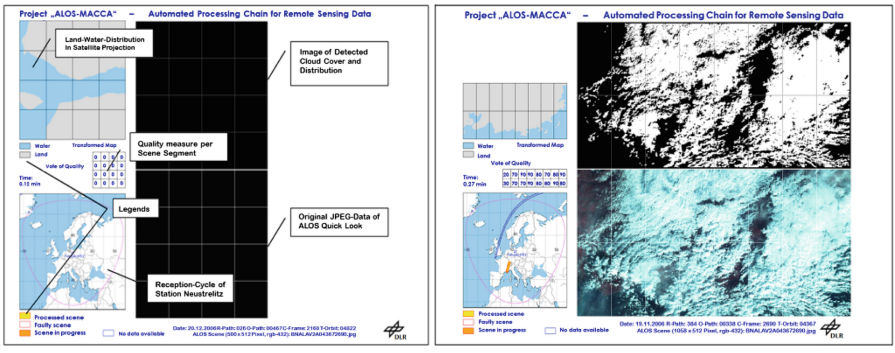

a) b)

Fig. 6. Result of data usability assessment of ALOS data (adopted and modified by [28]) (a) browse product with annotation of its parts, (b) sample of an ALOS browse product.

Additionally, the information about the data quality (comparison of votes by operator and automat are included) can be used as matrix to control the processing/post-processing of RS data within an automatic process chain.

An example for a browsable product supporting an interactive visual data usability assessment by interpreters/operators is given in Fig. 5. The product includes the transformed topographic map given in satellite perspective (top left), the satellite orbit with track and frame (bottom left) and the quick-look with red rendered clouds (right).

4 Conclusions

The demand for area-wide (large area covering) environmental information permanently increases. The provision of this information, based on EO data, only can be guaranteed by automatic and operative processing. In principle, the method developed for automated quality assessment of LANDSAT data can be applied to other satellite data. In addition, the algorithms were already generalized by e.g. including a varying size of the images and by adoption satellite systems with a tilting sensor, here namely for the ALOS sensor system (Fig. 6). Figure 6a explains the individual elements included in the browsable product of changing size of data. Figure 6b shows a sample of a real ALOS browse product.

The continuously increasing number of RS missions, sensors and different data set available, as well as the considerably improved computer power and storage performance, including the ongoing improvement of automation of RS interpretation offer new possibilities in value adding of RS data for diverse applications. The requirements of the ESA on the functionality of the introduced processor have shown the following aspects:

1. Generic and automated RS data interpretation providing near real time data information products for time-critical applications is a service that has to be realised urgently.
2. Nevertheless that the respective interpretation processor provides only a selected set of information, a high-level of accuracy has to be guaranteed.
3. The developed processor includes all essential modules needed for processing of tailored products providing information for the user.
4. The basic structure of the presented processing chain was used to derive dynamic land-water masks (MERIS-, AATSR-, VEGETATION-data) in the ESA CCI project “Burned Area”. A self-learning classification algorithm was developed for uncompressed data in order to derive the masks [31, 32].

Acknowledgement. The authors thank Dr. Berutti, Dr. Pitella, Dr. Biasutti (all European Space Agency) for the provided test data, for the constructive discussions, and the shown interest in our investigations. The authors wish to thanks E. Schwarz from the German Remote Date Center, Department of National Ground Segment Neustrelitz for his activities for determination of the actual equator crossing time.

References

1. EU. http://ec.europa.eu/enterprise/policies/space/gmes/. Accessed 06 Aug 2012
2. Borg, E., Fichtelmann, B., Asche, H.: Assessment for remote sensing data: accuracy of interactive data quality interpretation. In: Murgante, B., Gervasi, O., Iglesias, A., Taniar, D., Apduhan, B.O. (eds.) ICCSA 2011. LNCS, vol. 6783, pp. 366–375. Springer, Heidelberg (2011). doi:10.1007/978-3-642-21887-3_29
3. Borg, E., Fichtelmann, B., Asche, H.: Cloud classification in JPEG-compressed remote sensing data (LANDSAT 7/ETM +). In: Murgante, B., Gervasi, O., Misra, S., Nedjah, N., Rocha, A.M.A.C., Taniar, D., Apduhan, B.O. (eds.) ICCSA 2012. LNCS, vol. 7334, pp. 347–357. Springer, Heidelberg (2012). doi:10.1007/978-3-642-31075-1_26
4. Lau, W.-L., Li, Z.-L., Lam, K.W.-K.: Effects of JPEG compression on image classification. Int. J. Remote Sens. **24**(7), 1535–1544 (2003)
5. Berutti, V.: LANDSAT 7 ESA Stations Network Report - Focus on Product Generation, LTWG 11, LANDSAT Technical Working Group Meeting (USGS/NASA), Canberra, Australia, 4–8 February, 21 p. (2002)
6. Bettac, H.-D., Reiniger, K., Brieß, K., Borg, E.: DLR/DFD presentation to the LGSOWG-30 Meeting, LGSOWG Meeting, Orlando, Florida, USA, 12–15 November, 22 p. (2001)
7. Pollex, J.: Oral communication (2011)
8. Schwarz, J., Bettac, H.D., Missling, K.-D.: Das DFD-Bodensegment für LANDSAT-7, DLR-Mitteilung 1999–2003, Mehl, D. (Eds.), Wessling, Germany, 20–21 October, pp. 49–56 (2000)
9. Biasutti, R., 2000, *Cloud Cover Evaluation*, LTWG 8, LANDSAT Technical Working Group Meeting (USGS/NASA), Ottawa, Canada, July 17–22, 10 p
10. Richter, R., Schläpfer, D.: Atmospheric/Topographic Correction for Satellite Imagery. DLR, Wessling (2011). DLR report DLR-IB 565-02/11
11. Huang, L., Li, Z.: Feature-based image registration using the shape context. Int. J. Remote Sens. **31**(8), 2169–2177 (2010)
12. Borg, E., Fichtelmann, B., Böttcher, J., Günther, A., 2009, *Processing of remote sensing data*, EP 1 637 838 B1
13. Borg, E., Fichtelmann, B.: Verfahren und Vorrichtung zum Feststellen einer Nutzbarkeit von Fernerkundungsdaten, DP 10 2004 024 595 B3 (2004)
14. NASA 2011. http://landsathandbook.gsfc.nasa.gov/. Accessed 06 Aug 2012
15. Irish, R.: LANDSAT 7 Automatic Cloud Cover Assessment. In: Sylvia, D. (Eds.) Proceedings of SPIE (4049) Algorithms for Multispectral, Hyperspectral, and Ultraspectral Imagery VI, pp. 348–355 (2000)
16. Xu, Q., Wu, W.: ACRES Automatic Cloud Cover Assessment of LANDSAT 7 Images, Spatial Sciences Conference 2003 – Spatial Knowledge Without Boundaries Canberra, September 23–26, 10 p (2003)
17. Slater, P.N., Biggar, S.F., Holm, R.G., Jackson, R.D., Mao, Y., Moran, M.S., Palmer, J.M., Yuan, B.: Reflectance and radiance-based methods for the in-flight absolute calibration of multispectral sensors. Remote Sens. Environ. **22**, 11–37 (1987)
18. Markham, B.L., Barker, J.L.: Spectral characterization of the LANDSAT thematic mapper sensors. Int. J. Remote Sens. **6**, 697–716 (1985)
19. Chander, G., Markham, B.L., Helder, D.L.: Summary of current radiometric calibration coefficients for LANDSAT MSS, TM, ETM+, and EO-1 ALI sensors. Remote Sens. Environ. **113**, 893–903 (2009). http://landportal.gsfc.nasa.gov/Documents/Landsat_Calibration_Summary.pdf. Accessed 20 Feb 2012

20. Gurney, R.J., Hall, D.K.: Satellite-derived surface energy balance estimates in the Alaskan Sub-Arctic. J. Clim. Appl. Meteorol. **22**(1), 115–125 (1983)
21. MATHEMATIK, Kleine Enzyklopädie, Verlag Enzyklopädie, Leipzig (1970)
22. Johnson, D.B., Flament, P., Bernstein, R.L.: High-resolution satellite imagery for mesoscale meteorological studies. Bull. Am. Meteorol. Soc. **75**, 5–34 (1994)
23. Wu, Z.-J., McAvaney, B.: Sampling methods for climate model calculated brightness temperatures. BMRC Research Report No. 117, Bureau of Meteorology, Australia (2005)
24. Ignatov, A., Lazlo, I., Harrod, E.D., Kidwell, K.B., Goodrum, G.P.: Equator crossing times for NOAA, ERS and EOS sun-synchronous satellites. Int. J. Remote Sens. **25**, 5255–5266 (2004)
25. Bush, K.A., Smith, G.L., Young, D.F.: The NOAA-9 earth radiation budget experiment wide field-of-view data set. In: 10th Conference on Atmospheric Radiation, June 1999, NASA 1999 Technical Docs (1999)
26. Duffett-Smith, P.: Practical Astronomy with Your Calculator, 3rd edn. Cambridge University Press, Port Melbourne, Cambridge, Madrid) (1988)
27. Analytical Graphics, Inc. http://www.agi.com/
28. Fichtelmann, B., Borg, E., Kriegel, M.: Verfahren zur operationellen Bereitstellung von Zusatzdaten für die automatische Fernerkundungsdatenverarbeitung, 23. In: Salzburg, S. et al. (Eds.) AGIT-Symposium, pp. 12–20. Wichmann, Berlin, Offenbach (2011)
29. Lehmann, T., Oberschelp, W., Pelikan, E., Repges, R.: Bildverarbeitung für die Medizin-Grundlagen Modelle, Methoden, Anwendungen, p. 462. Springer, Heidelberg (1997)
30. Haberäcker, P.: Praxis der digitalen Bildverarbeitung und Mustererkennung. Hanser, München (1995)
31. Fichtelmann, B., Borg, E.: A new self-learning algorithm for dynamic classification of water bodies. In: Murgante, B., Gervasi, O., Misra, S., Nedjah, N., Rocha, A.M.A.C., Taniar, D., Apduhan, B.O. (eds.) ICCSA 2012. LNCS, vol. 7335, pp. 457–470. Springer, Heidelberg (2012). doi:10.1007/978-3-642-31137-6_35
32. Fichtelmann, B., Guenther, K.P., Borg, E.: Adaption of a self-learning algorithm for dynamic classification of water bodies to SPOT VEGETATION Data. In: Gervasi, O., Murgante, B., Misra, S., Gavrilova, M.L., Rocha, A.M.A.C., Torre, C., Taniar, D., Apduhan, B.O. (eds.) ICCSA 2015. LNCS, vol. 9158, pp. 177–192. Springer, Heidelberg (2015). doi:10.1007/978-3-319-21410-8_14

http://www.springer.com/978-3-319-51640-0

Leveraging Applications of Formal Methods, Verification, and Validation
6th International Symposium, ISoLA 2014, Corfu, Greece, October 8-11, 2014, and 5th International Symposium, ISoLA 2012, Heraklion, Crete, Greece, October 15-18, 2012, Revised Selected Papers
Lamprecht, A.-L. (Ed.)
2016, VII, 157 p. 62 illus., Softcover
ISBN: 978-3-319-51640-0